

Article

# Effect of Comminution Methods on Low-Rank Coal Bubble–Particle Attachment/Detachment: Implications for Flotation

Guoqiang Rong <sup>1,2</sup>, Yangchao Xia <sup>1,2,\*</sup>, Youfei Zhang <sup>1,2</sup>, Fangyu Guo <sup>1,2</sup>, Dongyue Wang <sup>3</sup>, Rui Zhang <sup>1,2</sup>, Yaowen Xing <sup>1,2,\*</sup> and Xiahui Gui <sup>1,2,4,\*</sup> 

<sup>1</sup> Chinese National Engineering Research Center of Coal Preparation and Purification, China University of Mining and Technology, Xuzhou 221116, China

<sup>2</sup> School of Chemical Engineering and Technology, China University of Mining and Technology, Xuzhou 221116, China

<sup>3</sup> School of Mineral Processing and Bioengineering, Central South University, Changsha 41000, China

<sup>4</sup> Henan Province Industrial Technology Research Institute of Resources and Materials, Zhengzhou University, Zhengzhou 450001, China

\* Correspondence: xiayangchao2010@163.com (Y.X.); cumtxyw@cumt.edu.cn (Y.X.); guixiahui1985@163.com (X.G.)

Received: 1 July 2019; Accepted: 18 July 2019; Published: 21 July 2019



**Abstract:** The floatability of fine low-rank coal particles can be greatly influenced by their morphological characteristics, such as shape and surface roughness. In this study, the attachment efficiency and detachment amplitude of fine low-rank coal particles produced by various comminution methods onto/from the bubble surface were investigated using homemade bubble–particle wrap angle and bubble–particle attachment/detachment testing systems. Results showed that the length–diameter ratio of rod-milled products was smaller than that of crushed products. The wrap angle of particles obtained by the crushed method was larger than that obtained by the rod-milled method, i.e., particles with greater length–diameter ratio showed higher attachment efficiency onto the bubble surface. Meanwhile, particles with greater length–diameter ratio exhibited a larger detachment amplitude, which suggests that it is more difficult to be detached from the bubble surface. However, rod-milled products showed lower attachment onto the bubble surface. The flotation test confirmed that the floatability ratio of crushed products was higher than that of rod-milled products, consistent with evidence from experimental analyses. This study provides a fundamental understanding of particle shapes for low-rank coal flotation by a novel research method combining the attachment efficiency and detachment amplitude of bubble–particle combinations.

**Keywords:** low-rank coal; floatability; particle shape; attachment efficiency; detachment amplitude

## 1. Introduction

Froth flotation, which utilizes the differences in floatability between valuable minerals and other particles, is the most economical mineral processing method used to separate fine mineral particles from gangue. With respect to the interaction between bubbles and particles in an aqueous solution, the flotation process is composed of three main sub-processes: collision, attachment, and detachment. The efficiencies of these sub-processes are responsible for the overall flotation efficiency [1–4]. The efficiency of collision is mostly affected by the hydrodynamic conditions of the flotation process, while the efficiency of bubble–particle attachment/detachment is very important for flotation. It should be noted that the attachment efficiency is largely influenced by the surface properties of mineral particles [2].

Meanwhile, the bubble–particle attachment is governed by surface morphological characteristics, such as the shape, surface roughness, and pores of particles [5–9].

The surface morphology of particles plays a key role in the floatability of minerals, such as coal, gold, chalcopyrite, pyrite, molybdenite, alumina, muscovite, talc, and quartz. The contact angle, pulp rheology, film stability of the particle surface, induction time for bubble–particle attachment, and mineral entrainment during flotation are significantly affected by the particle surface morphology. The rheology of chrysotile suspension is largely influenced by the shape of non-fibrous minerals and chrysotile fibers [10]. The ess-spherical bitumen molecules aggregate more easily [11]. The flattened gold particles are more likely to float and experience a higher recovery than cubic, spherical, or regular gold particles in gold flotation [12]. Angular chalcopyrite particles float faster than round ones in the absence of a collector. Talc and quartz particles with greater elongation and less roundness have higher floatability [13]. However, round pyrite particles have higher floatability than particles with a higher elongation ratio [14]. Irregular alumina and galena particles were observed to attach to the bubbles along their longest edges [15,16]. The disc-shaped ink and elongated quartz particles exhibit a larger contact area during bubble–particle attachment. This larger contact area reduces the rates of both thin film drainage and film rupturing [17–19]. Similarly, coal particles with less roundness float rapidly, whereas coal particles with more roundness float slowly [20]. Also, it is considered that the sharp edges of ground particles can easily trigger the film rupture process and shorten the attachment time [19,20].

However, the effect of the shape of particles obtained from different comminution methods on low-rank coal flotation has not been sufficiently studied. The length–diameter ratio can affect the floatability of various particles. In this study, the length–diameter ratio, wrap angle, bubble–particle attachment/detachment of rod-milled and crushed coal particles were investigated. The floatability ratio was calculated by performing a flotation experiment to verify the influence of comminution methods or shape on bubble–particle attachment/detachment.

## 2. Materials and Methods

### 2.1. Materials and Sample Preparation

The raw coal size was 0–13.00 mm, which was obtained from the Shendong Coal Mine, China. To ensure that the test sample was the new fine particle produced by two kinds of comminution equipment, the fine material of 0–0.50 mm in raw coal was screened out by pre-screening. The coal sample of 0.50–13.00 mm was fed into two comminution devices, one of which involved crushing using a hammer crusher while the other one consisted of wet grinding with a roll mill. The mass concentration of coal in the roll mill was 40%, and the sample was ground for 15 min. The single-stage open-circuit crushing process was adopted, and the discharged material was screened through two 0.50 mm and 0.25 mm sieves to sort out the 0.25–0.50 mm particles. The product of two comminution methods was used as a sample for each experiment and characterization in this study. During sample preparation, various factors were considered to ensure that the sample exhibited good consistency and representativeness. The flowsheet of sample preparation is shown in Figure 1.

### 2.2. Dynamic Image Particle Analysis

To investigate the morphology of the particles, shape measurements were carried out using the BT-2900 dynamic image particle analysis system (Figure 2), which performs 2D image analysis [21]. The BT-2900 image particle size analysis system consists of an electromagnetic vibration dynamic feeding system, a high-brightness LED array light source, an imported high-speed coupled-charged device (CCD), and a small phased-out lens. For grainy images shot randomly through a lens, computer software quickly identifies and processes the particles in real time, and displays the image, size, and shape data of each particle. The analysis result package includes the roundness and convexity of the particle morphology, reflecting particle size, particle size distribution, typical value, maximum particle size, specific range content, and less than or more than a certain particle size content. The

measuring range of particle size in this system is 0.03–10 mm. In this study, 1.5 g of crushed and rod-milled products (particle size of 0.5–0.25 mm) were used, with particle quantities of 13,562 and 13,667, respectively.

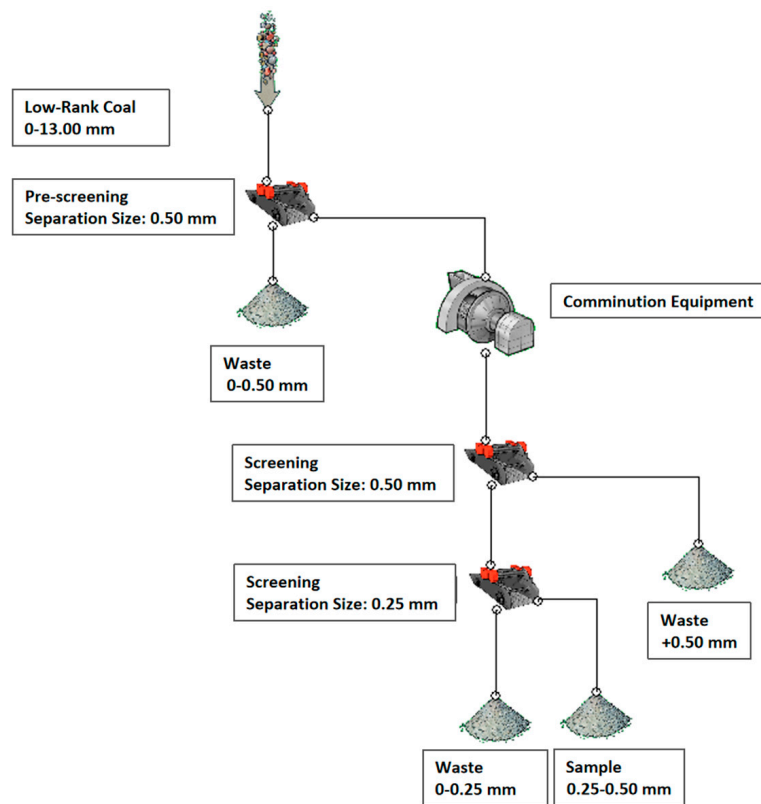


**Figure 1.** Flowsheet of sample preparation.

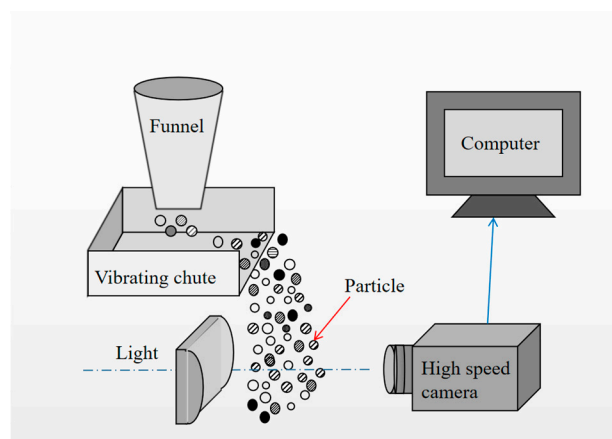


**Figure 2.** Schematic of the dynamic image particle analysis system.

### 2.3. Scanning Electron Microscopy (SEM)

The surface morphology of coal samples was determined by scanning electron microscopy (SEM; SIGMA, Carl Zeiss Company, Oberkochen, Germany). The coal samples were dried for 24 h in a vacuum drying chamber at 60 °C. After spraying gold on their surface, a 20 kV acceleration voltage was selected for SEM analysis.

#### 2.4. X-ray Photoelectron Spectrometry (XPS)

An X-ray photoelectron spectrometer (ESCALAB 250Xi, Thermo Scientific, Waltham, MA, USA) irradiated the samples with a beam of X-rays to analyze the elemental composition and chemical morphology of the sample surfaces. In the XPS spectra, elements and chemical states on the surface of the samples were determined from peak position and shape, and the content of the elements on the surface of the samples was determined from peak area. In this study, the chemical composition and chemical state of the synthesized samples were calibrated by the C1s peak value of 284.8 eV, using Al-K X-ray as the excitation source.

#### 2.5. Bubble–Particle Wrap Angle Experiment

The bubble–particle wrap angle (BPWA) was used to reveal coal floatability in low-rank coal flotation. A schematic of the bubble–particle wrap angle ( $\theta$ ) is shown in Figure 3. The BPWA experiment, used to simulate the flotation process and indicate the situation of particles attached to bubble surfaces, was first introduced by Chu et al. [22]. The BPWA defines the average coverage angle of the coal particles on the bubble surface and is directly connected to the floatability of coal particles. A larger BPWA means a better floatability [23].

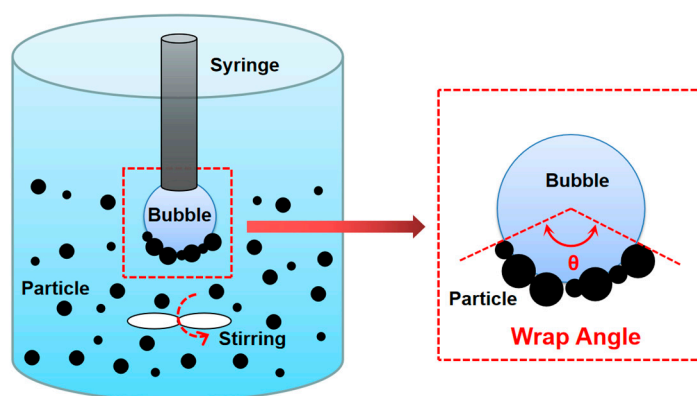


Figure 3. Schematic of bubble–particle wrap angle experiment.

A homemade BPWA experiment system was used in this study, in which 2 g of coal (particle size of 0.5–0.25 mm) was placed in a container with dimensions of  $5 \times 5 \times 10 \text{ cm}^3$ , together with 200 mL of ultrapure water. The diameter of the bubble was approximately 3.8 mm and the height between the center of the bubble and the bottom of the container was 50 mm. The rotor speed was set to 250 rpm. The stirring time was set to 40, 80, 120, 160, and 200 s, and bubble images were recorded accordingly.

#### 2.6. Bubble–Particle Attachment/Detachment Test

The bubble–particle attachment/detachment testing system, shown in Figure 4, was designed and assembled by our research team. The quantitative evaluation of bubble–particle attachment and detachment, e.g., the characterization of bubble induction time and detachment force, can be realized with a compact equipment structure and accurate test results [24].

The system includes a signal output unit, a motion drive unit, a bubble generation unit, a triaxial sample table and sample tank, a video monitoring unit, and a displacement acquisition unit. After the production of bubbles with consistent properties by the bubble generation unit, the triaxial sample table was used to adjust the relative position between the samples and bubbles. The signal output unit and motion drive unit completed the measurements of the properties of the particles, and the video monitoring unit and displacement acquisition unit performed the collection and storage of data.

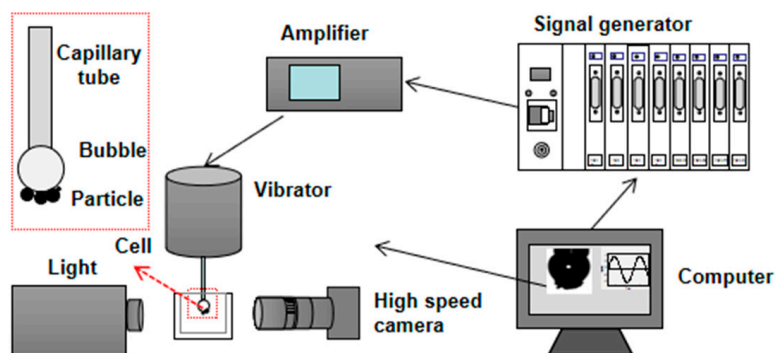


Figure 4. Schematic of the bubble–particle attachment/detachment testing system.

Bubble–particle detachment was investigated for various particle groups under different attachment modes. Low-rank coal samples with a particle size of 0.5–0.25 mm were selected, and a sinusoidal wave with a constant vibration frequency of 20 Hz and a constant bubble diameter of 3.8 mm were adopted. First, coal samples were placed in a glass tank, and the granular bed was kept flat and open. The light source and high-speed camera were adjusted to an appropriate position. An injection pump was used at the end of the stainless capillary to squeeze the bubble. A three-dimensional displacement platform was employed to form the coal particle bed. The rotor speed was set to 250 rpm. The bubble–particle group was obtained when the wrap angle was  $\sim 110^\circ$  after stirring, which is when the vibration began, and the amplitude was increased from 0 mm to the maximum. All the particles were detached from the bubble at the maximum critical detachment amplitude. During this period, images were recorded accordingly. The stability of the floc was evaluated using the maximum critical detachment amplitude. The maximum critical detachment amplitude is defined as the maximum driving amplitude with 50% detachment.

### 2.7. Flotation Procedure

Flotation tests were conducted in a 0.5 L flotation cell (XFD type flotation machine, Nanchang Jianfeng Mining Equipment Co., Ltd., Nanchang, China) using 40 g of coal sample with diesel oil as the collector and 2-octanol as the frother, both of which were analytical grade, purity >99%, and were purchased from the Sinopharm Chemical Reagent Co., Ltd., Nanjing, China. The dosages of the collector and frother were 1000 g/t coal and 500 g/t coal, respectively. The impeller speed of the flotation cell was 1800 rpm and the aeration rate was 0.25 m<sup>3</sup>/h. During the flotation process, 40 g of sample was first agitated with deionized water in a flotation cell for 2 min; the collector was then added and agitated for another 2 min. Next, the frother was added, and an additional 0.5 min of conditioning was maintained. Subsequently, air was introduced into the flotation cell, and the pulp was floated for 5 min.

## 3. Results and Discussion

### 3.1. Particle Shapes Analysis

With the dynamic particle image analysis system, the result of the length–diameter ratios of the crushed and rod-milled products is shown in Figure 4. The length–diameter (LD) ratio is defined as:

$$\text{LD ratio} = \frac{\text{length of particle}}{\text{diameter of particle}}$$

Figure 5 shows that the length–diameter ratios for the particles obtained from two types of comminution methods are different. The length–diameter ratio of rod-milled products is 2.101, whereas that of crushed products is 2.224, which means that rod-milled low-rank coal particles are closer to spherical particles, and crushed low-rank coal particles are closer to long strips.

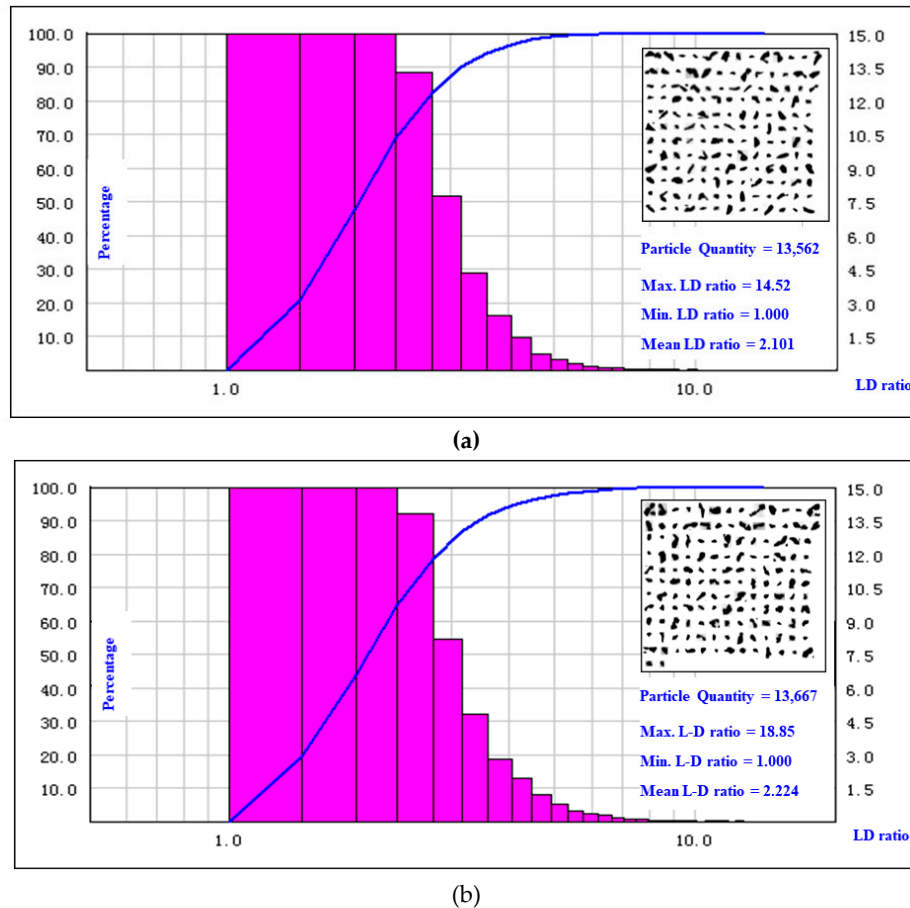


**Figure 5.** The length–diameter ratio of 0.5–0.25 mm low-rank coal particles: (a) rod-milled products, (b) crushed products.

### 3.2. SEM Results

SEM images of the coal samples of rod-milled and crushed products at different resolutions is shown in Figure 6. Figure 6a,b are the images of a rod-milled product at 300× and 4000× resolutions, while Figure 6c,d are the images of a crushed product at 300× and 4000× resolutions.

From Figure 6a,c, in the SEM images, the shape difference across comminution products is obvious. In the corresponding magnified images, Figure 6b,d, there is a certain degree of roughness. However, if enlarged 4000 times, there is not a great difference in the roughness between comminution products. The comminution method itself will not cause an obvious difference in the micro-morphology, but has a great influence on the whole particle shape, which is also the focus of this study.

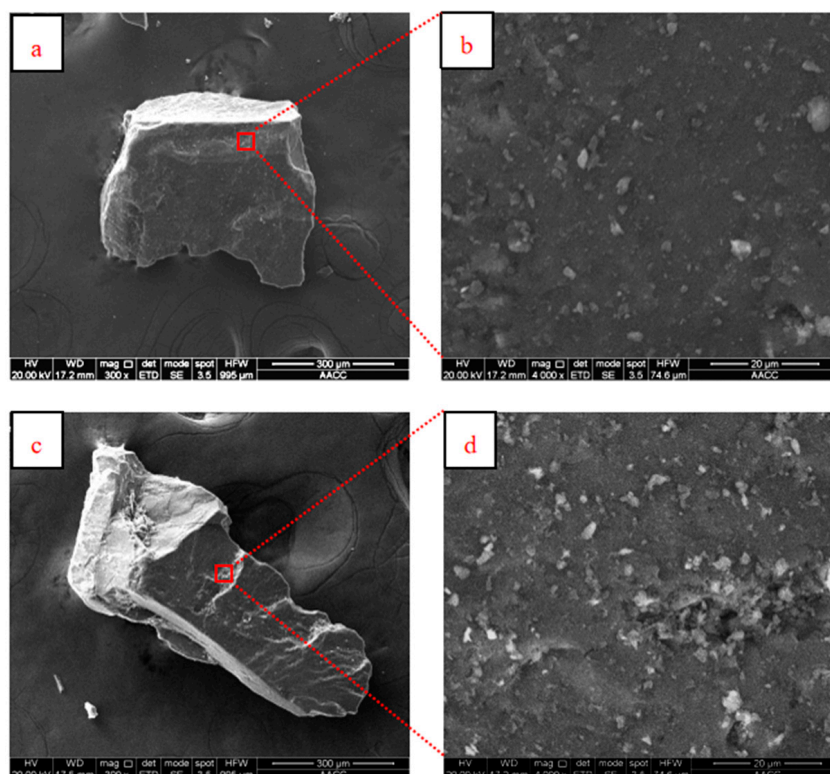


**Figure 6.** SEM images of different comminution products; (a) rod-milled products at 300 $\times$  resolutions, (b) rod-milled products at 4000 $\times$  resolutions, (c) crushed products at 300 $\times$  resolutions, (d) crushed products at 4000 $\times$  resolutions.

### 3.3. XPS Results

To reveal the effects of different comminution methods on oxygen functional groups and chemical composition on the surface of low-rank coal, X-ray photoelectron spectroscopy (XPS) analysis was carried out for rod-milled and crushed products. Figure 7 shows the XPS spectra of coal samples obtained by two different comminution methods. Eight characteristic peaks, such as those of C1s, O1s, Si2p, and Al2p, are observed in both spectra. The dominant structure of the C–C peaks in the two coal samples is evident, and the C–C bond in elemental C is 284.8 eV for correction.

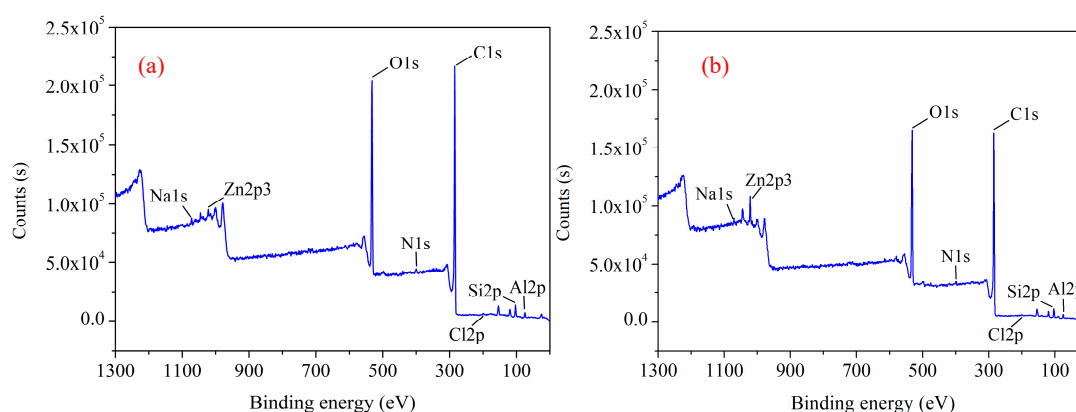


**Figure 7.** X-ray photoelectron spectroscopy (XPS) spectrum of different comminution products; (a) rod-milled products, (b) crushed products.

As shown in Figure 7 and Table 1, the difference in the main characteristic peaks of the products obtained by the two different grinding methods is less than 1.3%, which is very small. The contents

of surface carbon and oxygen were the main factors affecting surface wettability (hydrophobicity and hydrophilicity). Both the SEM and XPS tests indicated that the surface properties of the two comminution products, including roughness and wettability, were almost the same, which therefore would not have a significant effect on flotation. Thus, we investigated the effect of particle shape characteristics, such as the length–diameter ratio, on flotation.

**Table 1.** Atomic ratios of different comminution products.

Name	Atomic Ratio of Rod-Milled Products %	Atomic Ratio of Crushed Products %	Difference%
C1s	67.09	65.79	1.30
O1s	23.73	24.52	−0.79
Si2p	3.60	3.62	−0.02
Al2p	3.03	2.90	0.13
Na1s	0.59	0.00	0.59
N1s	1.23	2.13	−0.90
Cl2p	0.52	0.00	0.52
Zn2p3	0.21	1.04	−0.83

The difference of XPS spectra (Figure 7a,b) is caused by the difference of signal in instrument testing, so the content of the two samples cannot be directly judged from the spectrum, but the results of relative content testing can be used as a basis for direct judgment. The results show that the relative content of C1s and O1s from the rod-milled products is similar to that from the crushed products, with a difference of 1.30% and −0.79%, respectively.

#### 3.4. Bubble–Particle Wrap Angle Analysis

The wrap angle experiment simulated the attachment process between the particles and bubbles in the process of real flotation. As shown in Figure 8, the wrap angle of particles adhered to the surface of bubbles increases with increasing stirring time. Under the same stirring time, the wrap angle of crushed products is larger than that of the rod-milled products, which indicates that the crushed particles can be more easily attached to a bubble surface than rod-milled particles. In other words, the larger the length–diameter ratio of particles is, the higher the bubble–particle attachment efficiency is [25].

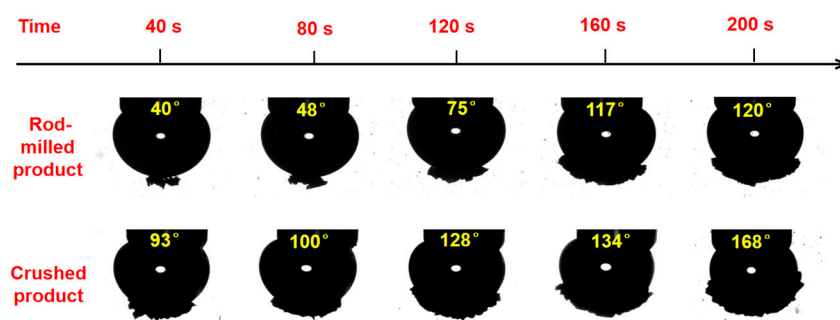


**Figure 8.** Wrap angles of low-rank coal particles (different comminution methods) adhered to the bubble surface for different stirring times.

#### 3.5. Bubble–Particle Attachment/Detachment Analysis

According to the study of Holtham and Cheng [26], the bubble–particle air floc under external force vibration can be regarded as a spring system. When the bubble–particle air floc vibrates, the motion of the air floc can be described as a simple sinusoidal motion. The velocity expression is as follows [27]:

$$V = -\omega A \sin(\omega t + \delta).$$

In the formula,  $\omega$  is the angular frequency,  $A$  is the amplitude,  $t$  is the time, and  $\delta$  is the vibration phase that determines the starting position of the sinusoidal wave. The acceleration of the vibration is shown as the formula below:

$$a_v = -\omega^2 A \cos(\omega t + \delta).$$

Therefore, the forces generated by vibration are shown as:

$$F_v = ma = -m\omega^2 A \cos(\omega t + \delta).$$

Thus, the expression of the maximum vibration force is:

$$F_{v,max} = m(2\pi f)^2 A.$$

In the vibration system, the detachment force of the particles is composed of the apparent gravity and vibration force. The maximum detachment force is expressed as:

$$F_{det,max} = (F_{v,max} + F'_g).$$

Because the apparent gravity of particles ( $F'_g$ ) is far less than the vibration force,  $F'_g$  is neglected. Therefore, the vibration force is considered to be the detachment force on the particles, which is expressed as:

$$F_{det,max} = m(2\pi f)^2 A.$$

In this formula,  $m$  is the particle mass,  $f$  is the vibration frequency, and  $A$  is the amplitude. Thus, the detachment force is determined by the amplitude when both the particle mass and the vibration frequency are fixed.

The bubble–particle detachment behavior of different comminution products was tested, and the analysis results are shown in Figure 9. It is shown that the maximum critical detachment amplitude of the rod-milled product is 1.344 mm, while that of the crushed product is 1.630 mm.

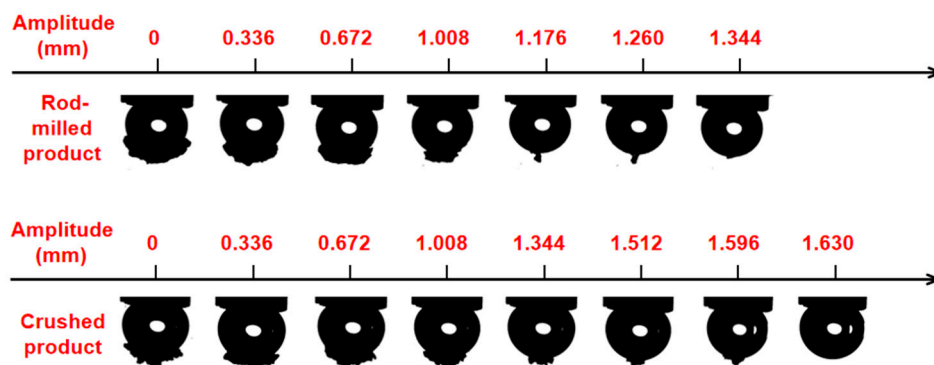


Figure 9. Bubble-particle detachment behavior of different comminution products.

The results show that rod-milled products are more likely to detach from bubbles than crushed ones, which results from the small length–diameter ratio and the short three-phase contact periphery; hence, the bubble–particle flocs are unstable. Crushed particles with irregular shape and large length–diameter ratio usually form a long three-phase contact periphery, which results in stronger adhesion and stronger stability of the bubble–particle floc. Hence, the large length–diameter particles obtained from the crushed method have a greater affinity for bubbles and are difficult to detach from the bubble surface. This phenomenon implies that the crushed method for low-rank coal is beneficial for coal flotation [25].

### 3.6. Flotation Results

As shown in Figure 5, the mean length–diameter ratio of rod-milled products was 2.101, whereas that of crushed products was 2.224. To verify the parameter of the length–diameter ratio on particle flotation, we defined the floatability ratio as:

$$\text{Floatability Ratio} = \frac{M_f}{M_s} \times 100\%$$

where  $M_f$  and  $M_s$  are the weights of the floats and sinks, respectively. As shown in Figure 10, the floatability ratio of crushed low-rank coal is 72%, which is higher than that of rod-milled low-rank coal with a floatability ratio of 58%. The floatability ratio is the comprehensive result of the bubble–particle attachment and detachment behavior. Combined with the results illustrated in Figures 7 and 8, we conclude that the coal particles from the crushed method with a larger length–diameter ratio show a higher floatability ratio than those obtained by the rod-milled method.

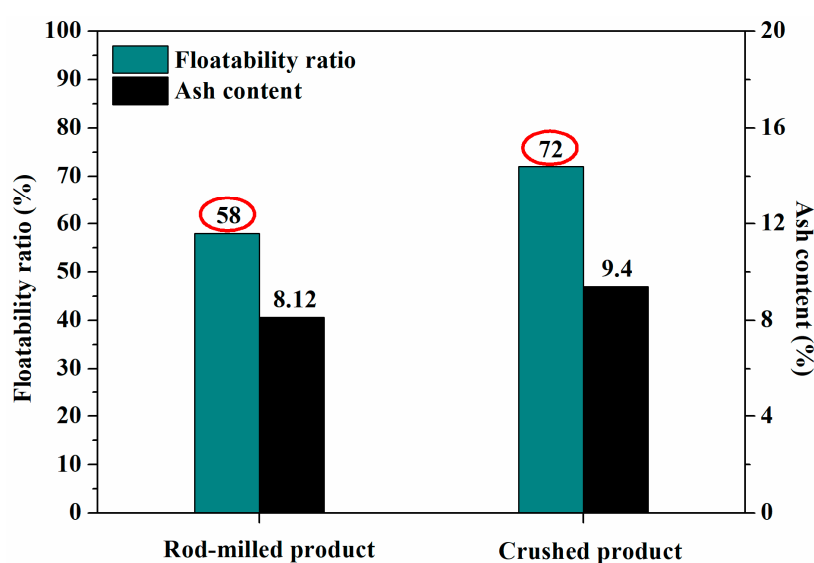


Figure 10. Floatability ratios of different comminution products.

## 4. Conclusions

The influence of the shape of fine low-rank coal particles produced by different comminution methods on bubble–particle attachment/detachment was investigated. It was found that the length–diameter ratio of rod-milled products was smaller than that of crushed products. The wrap angle of particles obtained by the crushed method was larger than that obtained by the rod-milled method; i.e., particles with greater length–diameter ratio showed higher attachment efficiency on the bubble surface. The maximum detachment amplitude of coal particle groups to the bubble was 1.630 mm, which corresponds to a large amplitude for crushed products, resulting in a more difficult detachment of particles from the bubble surface. However, the maximum detachment amplitude was 1.344 mm for coal particles of rod-milled products, exhibiting a lesser attachment onto the bubble surface. The flotation test showed that the floatability ratio of crushed products was higher than that of rod-milled products. The results also illustrated that coal particles from the crushed method with a larger length–diameter ratio show a higher floatability ratio than those obtained by the rod-milled method. This investigation provides a fundamental understanding of particle shapes for low-rank coal flotation by a novel research method combining attachment efficiency and detachment amplitude of bubble–particle combinations.

**Author Contributions:** Y.X. (Yangchao Xia) and G.R. conceived and designed the experiments; Y.Z., F.G., R.Z., and D.W. performed the experiments; X.G. and G.R. analyzed the data; Y.X. (Yaowen Xing) and G.R. wrote the paper.

**Funding:** This research was funded by National Key R&D Program of China (2018YFC0604702), Jiangsu Province Science Fund for Distinguished Young Scholars (BK20180032), the National Nature Science Foundation of China (Grant nos. 51774286, 51574236), the Postgraduate Research & Practice Innovation Program of Jiangsu Province (No. KYCX19\_2135), the Young Elite Scientists Sponsorship Program by CAST (2018QNRC001), the Postgraduate Research & Practice Innovation Program of China University of Mining and Technology (No. KYCX19\_2135), and the China Postdoctoral Science Foundation (2018M642369).

**Acknowledgments:** This work was supported by National Key R&D Program of China (2018YFC0604702), Jiangsu Province Science Fund for Distinguished Young Scholars (BK20180032), the National Nature Science Foundation of China (Grant nos. 51774286, 51574236), the Postgraduate Research & Practice Innovation Program of Jiangsu Province (No. KYCX19\_2135), the Young Elite Scientists Sponsorship Program by CAST (2018QNRC001), the Postgraduate Research & Practice Innovation Program of China University of Mining and Technology (No. KYCX19\_2135), and the China Postdoctoral Science Foundation (2018M642369), for which the authors express their appreciation.

**Conflicts of Interest:** The authors declare no conflict of interest.

## References

1. Nguyen, A.V.; Schulze, H.-J. *Colloidal Science of Flotation*; Marcel Dekker Inc.: New York, NY, USA, 2003.
2. Yoon, R.H. The role of hydrodynamic and surface forces in bubble–particle interaction. *Int. J. Miner. Process.* **2000**, *58*, 129–143. [[CrossRef](#)]
3. Xing, Y.; Xu, M.; Gui, X.; Cao, Y.; Babel, B.; Rudolph, M.; Weber, S.; Kappl, M.; Butt, H.J. The application of atomic force microscopy in mineral flotation. *Adv. Colloid Interface Sci.* **2018**, *256*, 373–392. [[CrossRef](#)]
4. Xing, Y.; Gui, X.; Pan, L.; Pinchasik, B.; Cao, Y.; Liu, J.; Kappl, M.; Butt, H.J. Recent experimental advances for understanding bubble–particle attachment in flotation. *Adv. Colloid Interface Sci.* **2017**, *246*, 105–132. [[CrossRef](#)]
5. Xia, Y.; Zhang, R.; Xing, Y.; Gui, X. Improving the adsorption of oily collector on the surface of low-rank coal during flotation using a cationic surfactant: an experimental and molecular dynamics simulation study. *Fuel* **2019**, *235*, 687–695. [[CrossRef](#)]
6. Guven, O.; Ozdemir, O.; Karaagaciloglu, I.E.; Çelika, M.S. Surface morphologies and floatability of sand-blasted quartz particles. *Miner. Eng.* **2015**, *70*, 1–7. [[CrossRef](#)]
7. Hassas, B.V.; Caliskan, H.; Guven, O.; Karakas, F.; Cinar, M.; Celik, M.S. Effect of roughness and shape factor on flotation characteristics of glass beads. *Colloids Surf. A Physicochem. Eng. Asp.* **2016**, *492*, 88–99. [[CrossRef](#)]
8. Koh, P.T.; Verrelli, D.I. Influence of particle shape on flotation performance. In *XXVII International Mineral Processing Congress (IMPC 2014)*; Yianatos, J., Ed.; U. de Chile/U. de Concepción/UTFSM/Colegio de Ingenieros de Chile/Gecamin: Santiago, Chile, 2014.
9. Verrelli, D.I.; Bruckard, W.J.; Koh, P.T.L.; Schwarz, M.P.; Follink, B. Influence of particle shape and roughness on the induction period for particle–bubble attachment. In *XXVI International Mineral Processing Congress (IMPC 2012)*; Indian Institute of Mineral Engineers (IIME) and Indian Institute of Metals (IIM): New Delhi, India, 2012; p. 2012.
10. Verrelli, D.I.; Bruckard, W.J.; Koh, P.T.L.; Schwarz, M.P.; Follink, B. Particle shape effects in flotation. Part 1: Microscale experimental observations. *Miner. Eng.* **2014**, *58*, 80–89. [[CrossRef](#)]
11. Xia, Y.; Yang, Z.; Zhang, R.; Xing, Y.; Gui, X. Enhancement of the surface hydrophobicity of low-rank coal by adsorbing DTAB: An experimental and molecular dynamics simulation study. *Fuel* **2019**, *239*, 145–152. [[CrossRef](#)]
12. Ndlovu, B.N.; Forbes, E.; Becker, M.; Deglon, D.A.; Franzidis, J.P.; Laskowski, J.S. The effects of chrysotile mineralogical properties on the rheology of chrysotile suspensions. *Miner. Eng.* **2011**, *24*, 1004–1009. [[CrossRef](#)]
13. Ng, S.; Warszynski, P.; Zembala, M.; Malysa, K. Bitumen-air aggregates flow to froth layer: II. Effect of ore grade and operating conditions on aggregate composition and bitumen recovery. *Miner. Eng.* **2000**, *13*, 1519–1532. [[CrossRef](#)]
14. Allan, G.C.; Woodcock, J.T. A review of the flotation of native gold and electrum. *Miner. Eng.* **2001**, *14*, 931–962. [[CrossRef](#)]
15. Hiçyilmaz, C.; Ulusoy, U.; Yekeler, M. Effects of the shape properties of talc and quartz particles on the wettability based separation processes. *Appl. Surf. Sci.* **2004**, *233*, 204–212. [[CrossRef](#)]

16. Vizcarra, T.G.; Harmer, S.L.; Wightman, E.M.; Johnson, N.W.; Manlapig, E.V. The influence of particle shape properties and associated surface chemistry on the flotation kinetics of chalcopyrite. *Miner. Eng.* **2011**, *24*, 807–816. [[CrossRef](#)]
17. Guven, O.; Karakas, F.R.; Kodrazi, N.; Elik, M.S. Dependence of morphology on anionic flotation of alumina. *Int. J. Miner. Process.* **2016**, *156*, 69–74. [[CrossRef](#)]
18. Aslani, M.R.; Rezai, B. Influence of particles shape characteristics of galena on their flotability under the flotation behavior. In Proceedings of the 8th International Scientific Conference on Modern Management of Mine Producing, Geology and Environmental Protection (SGEM), Albena, Bulgaria, 16–20 June 2008; Volume 1, pp. 457–464.
19. Schmidt, D.C.; Berg, J.C. Selective removal of toner particles from repulped slurries by flotation. *Pulp Pap. Can.* **1997**, *98*, 21–24.
20. Ulusoy, U.; Yekeler, M.; Hiçyılmaz, C. Determination of the shape, morphological and wettability properties of quartz and their correlations. *Miner. Eng.* **2003**, *16*, 951–964. [[CrossRef](#)]
21. Oliver, J.P.; Huh, C.; Mason, S.G. An experimental study of some effects of solid surface roughness on wetting. *Colloids Surf.* **1980**, *1*, 79–104. [[CrossRef](#)]
22. Szczerkowska, S.; Wiertel-Pochopien, A.; Zawala, J.; Larsen, E.; Kowalczyk, P.B. Kinetics of froth flotation of naturally hydrophobic solids with different shapes. *Miner. Eng.* **2018**, *121*, 90–99. [[CrossRef](#)]
23. Ulusoy, U.; Kursun, I. Comparison of different 2D image analysis measurement techniques for the shape of talc particles produced by different media milling. *Miner. Eng.* **2011**, *24*, 91–97. [[CrossRef](#)]
24. Chu, P.; Mirnzwami, M.; Finch, J.A. Quantifying particle pick up at a pendant bubble: A study of non-hydrophobic particle–bubble interaction. *Miner. Eng.* **2014**, *55*, 162–164. [[CrossRef](#)]
25. Xia, Y.; Wang, L.; Zhang, R.; Yang, Z.; Xing, Y.; Gui, X.; Cao, Y.; Sun, W. Enhancement of flotation response of fine low-rank coal using positively charged microbubbles. *Fuel* **2019**, *245*, 505–513. [[CrossRef](#)]
26. Holtham, P.N.; Cheng, T.W. Study of probability of detachment of particles from bubbles in flotation. *Trans. Inst. Min. Metall. Sect. C* **1991**, *100*, 147–153.
27. Xu, D.; Ametov, I.; Grano, S.R. Detachment of coarse particles from oscillating bubbles—The effect of particle contact angle, shape and medium viscosity. *Int. J. Miner. Process.* **2011**, *101*, 50–57. [[CrossRef](#)]



© 2019 by the authors. Licensee MDPI, Basel, Switzerland. This article is an open access article distributed under the terms and conditions of the Creative Commons Attribution (CC BY) license (<http://creativecommons.org/licenses/by/4.0/>).